



UNIVERSITY OF LEEDS

This is a repository copy of *Optically pumped intersublevel midinfrared lasers based on InAs-GaAs quantum dots* .

White Rose Research Online URL for this paper:
<http://eprints.whiterose.ac.uk/1119/>

Article:

Vukmirovic, N., Ikonc, Z., Jovanovic, V.D. et al. (2 more authors) (2005) Optically pumped intersublevel midinfrared lasers based on InAs-GaAs quantum dots. *IEEE Journal of Quantum Electronics*, 41 (11). pp. 1361-1368. ISSN 0018-9197

<https://doi.org/10.1109/JQE.2005.856077>

Reuse

See Attached

Takedown

If you consider content in White Rose Research Online to be in breach of UK law, please notify us by emailing eprints@whiterose.ac.uk including the URL of the record and the reason for the withdrawal request.



eprints@whiterose.ac.uk
<https://eprints.whiterose.ac.uk/>

Optically Pumped Intersublevel MidInfrared Lasers Based on InAs–GaAs Quantum Dots

Nenad Vukmirović, *Student Member, IEEE*, Zoran Ikonić, Vladimir D. Jovanović, Dragan Indjin, and Paul Harrison, *Senior Member, IEEE*

Abstract—We propose an optically pumped laser based on intersublevel transitions in InAs–GaAs pyramidal self-assembled quantum dots. A theoretical rate equations model of the laser is given in order to predict the dependence of the gain on pumping flux and temperature. The energy levels and wave functions were calculated using the 8-band $k \cdot p$ method where the symmetry of the pyramid was exploited to reduce the computational complexity. Carrier dynamics in the laser were modeled by taking both electron-longitudinal optical phonon and electron-longitudinal acoustic phonon interactions into account. The proposed laser emits at $14.6 \mu\text{m}$ with a gain of $g \approx 570 \text{ cm}^{-1}$ at the pumping flux $\Phi = 10^{24} \text{ cm}^{-2} \text{ s}^{-1}$ and a temperature of $T = 77 \text{ K}$. By varying the size of the investigated dots, laser emission in the spectral range $13\text{--}21 \mu\text{m}$ is predicted. In comparison to optically pumped lasers based on quantum wells, an advantage of the proposed type of laser is a lower pumping flux, due to the longer carrier lifetime in quantum dots, and also that both surface and edge emission are possible. The appropriate waveguide and cavity designs are presented, and by comparing the calculated values of the gain with the estimated losses, lasing is predicted even at room temperature for all the quantum dots investigated.

Index Terms—Intraband transitions, mid-infrared, optically pumped lasers, quantum dots.

I. INTRODUCTION

INTRABAND optical transitions in semiconductor nanostructures are a subject of intensive research due to their applications for sources and detectors of mid and far-infrared radiation. In quantum-well-based intersubband lasers, such as quantum cascade lasers [1], [2] and optically pumped lasers [3]–[6], the lasing threshold depends on the lifetime of the upper laser level which is determined by longitudinal-optical (LO) phonon scattering and is of the order of picoseconds. In order to have a lower threshold, LO-phonon scattering needs to be reduced.

Due to the discrete nature of states in quantum dots, electron relaxation due to the interaction with LO-phonons has previously been considered to be vanishingly small unless the energy levels are separated by the energy of an LO-phonon. Consequently, a quantum-dot cascade laser with six orders of magnitude lower threshold current than in quantum-well-based devices was expected [7]. However, current thought is that the electron-LO-phonon interaction in quantum dots should be

considered in the strong coupling regime [8], [9] and theoretical predictions of relaxation due to LO-phonon decay [10], [11] have indicated relaxation times of the order of hundred of picoseconds, in accordance with experimentally measured values [12], [13]. This is still two orders of magnitude larger than in quantum wells and the latest theoretical proposals of quantum-dot cascade lasers [14]–[16] predict low threshold currents, as well. Recently, electroluminescence from such structures has been observed [17], [18].

On the other hand, to the best of our knowledge, the possibility of having an optically pumped laser based on intersublevel transitions in quantum dots has not yet been analyzed. In this paper, we present the first theoretical proposal of such a laser based on pyramidal InAs–GaAs quantum dots, emitting at $\lambda \approx 14.6 \mu\text{m}$. In comparison to similar lasers based on quantum wells, the proposed laser has the advantage that in-plane polarized emission is possible and a lower pumping flux is needed due to the longer carrier lifetimes in quantum dots.

This paper is organized as follows. In Section II, we give a theoretical model of the laser active region. In Section III, the calculation of the pumping flux and temperature dependence of the gain is presented and appropriate waveguides for both edge and surface emission are designed.

II. THEORETICAL MODEL

A. Electronic Structure of Pyramidal Self-Assembled InAs–GaAs Quantum Dots

The method for calculation of energy levels and wave functions in pyramidal InAs–GaAs quantum dots is based on exploiting the \bar{C}_4 symmetry of the 8-band $k \cdot p$ Hamiltonian. It has been described in detail elsewhere [19] and only a brief review is given here.

The 8-band $k \cdot p$ Hamiltonian in the presence of strain [20] was used to calculate the energy levels in the conduction band. The strain distribution was taken into account via the continuum mechanical model. The plane wave method [21] was used to solve the Hamiltonian eigenvalue problem, therefore, only the Fourier transforms of the strain components given by analytical formulae in [22] are necessary. The plane wave method is based on embedding the quantum dot in a box of sides L_x , L_y and L_z and assuming the envelope functions $\psi_l(\mathbf{r})$ ($l \in \{1, 2, \dots, 8\}$) are linear combinations of plane waves

$$\psi_l(\mathbf{r}) = \sum_{\mathbf{k}} A_{l,\mathbf{k}} \exp(i\mathbf{k} \cdot \mathbf{r}) \quad (1)$$

Manuscript received June 18, 2005; revised July 19, 2005.

The authors are with the Institute of Microwaves and Photonics, School of Electronic and Electrical Engineering, University of Leeds, Leeds LS2 9JT, U.K. (e-mail: eennv@leeds.ac.uk).

Digital Object Identifier 10.1109/JQE.2005.856077

TABLE I
CALCULATED VALUES OF THE PUMP λ_p AND THE EMISSION WAVELENGTH λ_e , GAIN g_{77} AT THE TEMPERATURE OF $T = 77$ K AND g_{300} AT $T = 300$ K, AT THE PUMPING FLUX $\Phi = 10^{24}$ $\text{cm}^{-2} \text{s}^{-1}$ FOR SEVERAL DIFFERENT QUANTUM DOTS. THE WIDTH OF THE QUANTUM-DOT BASE IS b AND THE HEIGHT h

b [nm]	h [nm]	λ_p [μm]	λ_e [μm]	g_{77} [cm^{-1}]	g_{300} [cm^{-1}]
14	6	5.7	13.5	513	218
15	7	5.9	14.6	574	243
16	8	6.2	15.5	577	186
17	8.5	6.5	16.5	561	167
18	9	6.8	17.6	577	211
19	9.5	7.1	18.9	537	202
20	10	7.4	20.1	441	170

with the coefficients $A_{l,\mathbf{k}}$ to be determined. The wave vectors taken in the summation are given by

$$\mathbf{k} = 2\pi \left(\frac{m_x}{L_x}, \frac{m_y}{L_y}, \frac{m_z}{L_z} \right) \quad (2)$$

($m_x \in \{-n_x, \dots, n_x\}, m_y \in \{-n_y, \dots, n_y\}, m_z \in \{-n_z, \dots, n_z\}$). A direct application of the plane wave approach would deliver an $N \times N$ matrix, where N is the number of plane waves taken. However, it is possible to exploit the symmetry of the system to block diagonalize the corresponding matrix. The group projector method was used to find the symmetry adapted basis. In this basis the Hamiltonian matrix is block diagonal with four blocks of approximately equal size. The states are characterized by the total quasi-angular momentum quantum number $m_f \in \{-3/2, -1/2, 1/2, 3/2\}$ according to the irreducible representation A_{m_f} they belong to. The small piezoelectric potential that reduces the symmetry from \bar{C}_4 to \bar{C}_2 was treated as a perturbation.

The dependence of the positions of the first seven energy levels on dot size for quantum dots considered in this work (whose dimensions are given in Table I) is shown in Fig. 1.

As already pointed out by other workers [21], the plane wave method is very convenient for modeling the optical properties and carrier dynamics in quantum-dot structures. This is due to the fact that matrix elements can be expressed analytically in terms of the coefficients in the plane wave expansion, in contrast to other methods where numerical three-dimensional integration would be necessary.

B. Interaction With Electromagnetic Radiation

The Hamiltonian \hat{H}' of the interaction with the electromagnetic field is obtained by replacing \mathbf{k} with $\mathbf{k} + (e/\hbar)\mathbf{A}$ in the kinetic part \hat{H}_k of the $k \cdot p$ Hamiltonian [23] (where $\mathbf{A} = A\boldsymbol{\varepsilon}$ is the magnetic vector potential, $\boldsymbol{\varepsilon}$ is the polarization vector of the radiation, e is the elementary charge and \hbar the reduced Planck's constant), i.e., $\hat{H}' = \hat{H}_k(\mathbf{k} + (e/\hbar)\mathbf{A}) - \hat{H}_k(\mathbf{k})$. In the dipole approximation \mathbf{A} is considered constant in space, and furthermore all the terms quadratic in \mathbf{A} are neglected.

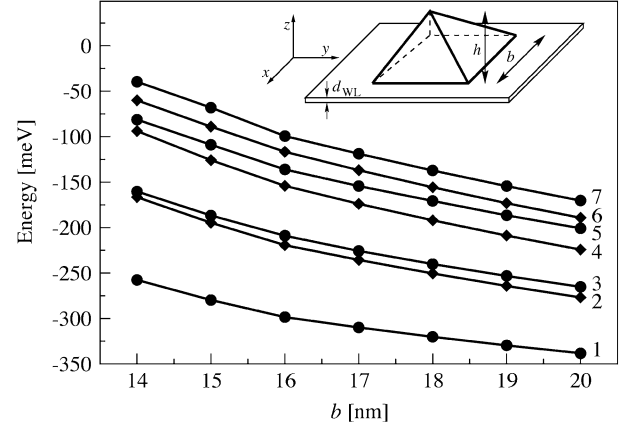


Fig. 1. Dependence of the first seven energy levels on dot size for quantum dots whose dimensions are given in Table I. The unstrained GaAs conduction band edge was taken as the reference energy level. The states with the quantum number $m_f = \pm 1/2$ are represented with circles and states with $m_f = \pm 3/2$ with diamonds. Lines are given only as a guide to the eye. The inset: quantum dot geometry. The base width is b , the height h , the wetting layer width d_{WL} .

According to Fermi's Golden rule, the transition rate from an initial state $|i\rangle$ to a final state $|f\rangle$ due to interaction with electromagnetic radiation of angular frequency ω is given by

$$W_{if} = \frac{2\pi}{\hbar} |\langle i | \hat{H}' | f \rangle|^2 \delta(E_f - E_i \mp \hbar\omega) \quad (3)$$

where the “-” sign corresponds to absorption and “+” to emission, and E_f and E_i are the energies of the final and initial state, respectively.

The inhomogeneous broadening due to size inhomogeneity of the quantum-dot ensemble was taken into account by replacing the delta function with a Gaussian, i.e.,

$$\delta(x) \rightarrow g(x, 2\sigma) = \frac{1}{\sigma\sqrt{2\pi}} \exp\left(-\frac{x^2}{2\sigma^2}\right). \quad (4)$$

The width 2σ was taken equal to 12% of the transition energy, which is a typical value in quantum-dot infrared photodetectors based on bound-to-bound transitions [24], [25]. The optical cross section of the $i \rightarrow f$ transition is given by $\sigma_{if} = W_{if}/\Phi$, where Φ is the optical pump flux. Using the relation between the flux and the vector potential one has

$$\sigma_{if}^{\boldsymbol{\varepsilon}}(\omega) = \frac{2\pi}{\bar{n}\varepsilon_0 c \omega} |\mathcal{M}_{if}^{\boldsymbol{\varepsilon}}|^2 g(E_f - E_i \mp \hbar\omega, 2\sigma) \quad (5)$$

where \bar{n} is the refraction index, c the speed of light in vacuum and ε_0 the vacuum dielectric constant. $\mathcal{M}_{if}^{\boldsymbol{\varepsilon}} = \langle i | \hat{H}' | f \rangle / A$ is the matrix element which depends only on the direction $\boldsymbol{\varepsilon}$ of light polarization and not on the amplitude of A . With the envelope functions of the final and initial state given by

$$\psi_j^{f(i)}(\mathbf{r}) = \sum_{\mathbf{k}} A_{j,\mathbf{k}}^{f(i)} \exp(i\mathbf{k} \cdot \mathbf{r}) \quad (6)$$

the matrix element is equal to

$$\mathcal{M}_{if}^{\boldsymbol{\varepsilon}} = V \sum_{l,\mathbf{q}} \sum_{j,\mathbf{k}} A_{l,\mathbf{q}}^{i*} A_{j,\mathbf{k}}^f G_{lj}(\mathbf{q}, \mathbf{k}) \quad (7)$$

where $V = L_x L_y L_z$ is the volume of the embedding box and

$$G_{lj}(\mathbf{q}, \mathbf{k}) = \frac{1}{AV} \int_V d^3\mathbf{r} \exp(-i\mathbf{q} \cdot \mathbf{r}) H'_{lj} \exp(i\mathbf{k} \cdot \mathbf{r}) \quad (8)$$

are the Fourier transforms of the perturbation Hamiltonian matrix elements. They can all be expressed analytically in terms of the components of the vectors \mathbf{k} , \mathbf{q} , and $\boldsymbol{\varepsilon}$, the material parameters of InAs and GaAs and the Fourier transform of the quantum-dot characteristic function (see [19] or [22] for its definition). The same recipe as in [19] for the order of differential and multiplication operators was used to ensure the hermiticity of the perturbation Hamiltonian matrix.

After calculating the matrix elements between states with a well defined symmetry, we find the selection rules: $\Delta m_f = 0$ for z -polarized light and $\Delta m_f = \pm 1$ for in-plane polarized light (where by the definition $3/2 + 1 = -3/2$ and $-3/2 - 1 = 3/2$). These are analogous to selection rules in cylindrically symmetric systems, despite the fact that pyramidal dots have a lower symmetry.

C. Carrier Dynamics in a Quantum Dot

In this subsection, we examine the processes which lead to electron transitions between different energy levels. We give the relations for transition rates due to interaction with LO and longitudinal-acoustic (LA) phonons, as well as due to spontaneous emission. Electron-hole scattering which is considered to be the dominant mechanism in interband quantum-dot lasers [26] is not present in this unipolar device. Since we assume that the electrons are excited to only bound states (this assumption will be justified in Section III), the relaxation processes assisted by the Coulomb interaction between bound and wetting layer carriers [27] do not exist as well. Consequently, the electron-electron interaction has no effect on rate equations, because due to energy conservation the transition of an electron from state i to state f must be compensated by the transition of another electron from state f to state i .

1) *Interaction With LO Phonons:* The electron–LO–phonon interaction was considered in the strong coupling regime where the carrier lifetime is determined by the decay of an LO-phonon into two LA-phonons [10]. The transition rate from the initial state $|\Psi_i; \{n_{\mathbf{q}}\}\rangle$ with an electron in state i and $n_{\mathbf{q}}$ LO-phonons with the wave vector \mathbf{q} (where \mathbf{q} takes all possible values of the phonon wave vector) to the final state $|\Psi_f; \{n_{\mathbf{q}} \pm \delta_{\mathbf{q}, \mathbf{k}}\}\rangle$ with an electron in state f and one more (less) phonon with the wave vector \mathbf{k} is given by [10]

$$W_{if} = \Gamma - \frac{\sqrt{2(R-X)}}{\hbar} \quad (9)$$

where $R = \sqrt{X^2 + Y^2}$, $X = g^2 + (\Delta_{if}^2 - \Gamma^2 \hbar^2)/4$, $Y = \Gamma \hbar \Delta_{if}/2$, $\Delta_{if} = E_i - E_f \mp \hbar \omega_{LO}$, $g^2 = \sum_{\mathbf{k}} |g_{\mathbf{k}}|^2$ electron-LO-phonon coupling strength, where

$$g_{\mathbf{k}} = \langle \Psi_i; \{n_{\mathbf{q}}\} | \hat{H}_{e-ph} | \Psi_f; \{n_{\mathbf{q}} \pm \delta_{\mathbf{q}, \mathbf{k}}\} \rangle \quad (10)$$

$\hbar \omega_{LO}$ is the LO-phonon energy and Γ is the inverse LO-phonon lifetime due to its decay into two LA-phonons. Since Γ is weakly dependent on the phonon wave vector [28], this dependence was neglected. As it is thought that the influence of phonon confinement on scattering rates is not so important in AlGaAs–GaAs and InGaAs–GaAs nanostructures [29], we

have assumed bulk GaAs LO-phonon modes and correspondingly the Frölich interaction Hamiltonian is given by

$$\hat{H}_{e-ph} = \sum_{\mathbf{q}} (\alpha(\mathbf{q}) \hat{a}_{\mathbf{q}} e^{i\mathbf{q}\cdot\mathbf{r}} + \alpha(\mathbf{q})^* \hat{a}_{\mathbf{q}}^{\dagger} e^{-i\mathbf{q}\cdot\mathbf{r}}) \quad (11)$$

where $\hat{a}_{\mathbf{q}}$ and $\hat{a}_{\mathbf{q}}^{\dagger}$ are the phonon annihilation and creation operators and

$$|\alpha(\mathbf{q})| = \frac{1}{q} \sqrt{\frac{e^2 \hbar \omega_{LO}}{2V} \left(\frac{1}{\varepsilon_{\infty}} - \frac{1}{\varepsilon_{st}} \right)} \quad (12)$$

with ε_{∞} and ε_{st} being high frequency and static dielectric constants, respectively. From (10)–(12) one obtains

$$g^2 = \sum_{\mathbf{k}} (n_{\mathbf{k}} + 1/2 \pm 1/2) |\alpha(\mathbf{k})|^2 |F_{if}(\mathbf{k})|^2 \quad (13)$$

where

$$F_{if}(\mathbf{q}) = \sum_{j=1}^8 \int_V d^3\mathbf{r} \psi_j^f(\mathbf{r})^* e^{i\mathbf{q}\cdot\mathbf{r}} \psi_j^i(\mathbf{r}) \quad (14)$$

is the electron–phonon interaction form-factor. The summation in (13) is performed over phonon wave vectors given by (2). For such values of wave vectors the form-factor can be simplified to

$$F_{if}(\mathbf{q}) = V \sum_{j=1}^8 \sum_{\mathbf{k}_i} A_{j, \mathbf{k}_i + \mathbf{q}}^{f*} A_{j, \mathbf{k}_i}^i \quad (15)$$

Some of the calculated LO phonon interaction transition rates for quantum dots whose dimensions are given in Table I, are shown in Fig. 2.

2) *Interaction With LA Phonons:* The weaker electron-LA-phonon scattering was calculated using Fermi's Golden rule. The Hamiltonian of interaction with acoustic phonons is given by the same formula (11) except that in this case

$$|\alpha(\mathbf{q})| = \sqrt{\frac{D_A^2 \hbar q}{2\rho v_s V}} \quad (16)$$

where D_A is the acoustic phonon deformation potential, ρ the density and v_s the longitudinal sound velocity. The linear and isotropic acoustic phonon dispersion relation $\omega(\mathbf{q}) = v_s q$ is assumed. The transition rate from an initial state i to a final state f is then given by [30]

$$W_{if} = \Theta(\pm(E_i - E_f)) (n_{\mathbf{q}_s} + 1/2 \pm 1/2) \frac{D_A^2 q_s^3}{\hbar \rho v_s^2} \times \int \sin \theta d\theta d\varphi |F_{if}(\mathbf{q}_s)|^2 \quad (17)$$

where $q_s = |E_i - E_f|/(\hbar v_s)$, $\Theta(x)$ is the step function and (θ, φ) are the polar coordinates of the vector \mathbf{q}_s .

Acoustic phonon scattering is only significant when the states are closely spaced in energy (< 10 meV), as for example are

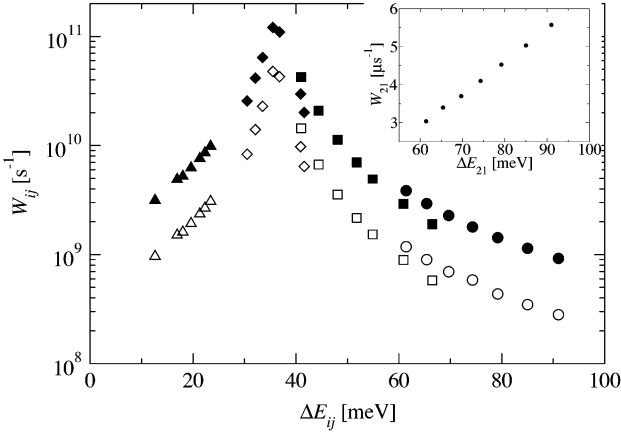


Fig. 2. Energy dependence of the calculated LO-phonon interaction transition rates W_{ij} on the transitions: $2 \rightarrow 1$ at $T = 77$ K (circles) and $T = 300$ K (full circles), $4 \rightarrow 3$ at $T = 77$ K (squares) and $T = 300$ K (full squares), $7 \rightarrow 5$ at $T = 77$ K (diamonds) and $T = 300$ K (full diamonds), $5 \rightarrow 4$ at $T = 77$ K (triangles) and $T = 300$ K (full triangles) for quantum dots whose dimensions are given in Table I. The inset: energy dependence of spontaneous radiative emission rate on the transition $2 \rightarrow 1$.

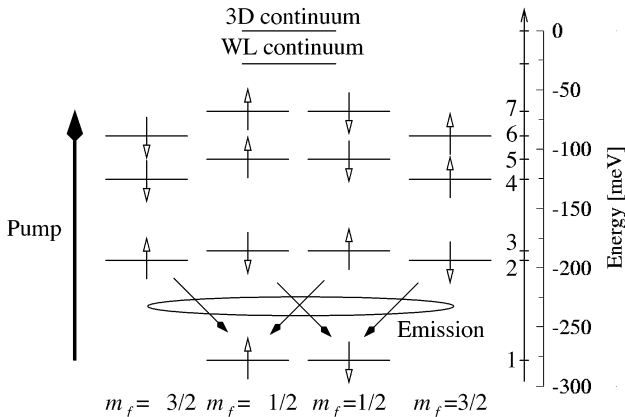


Fig. 3. Scheme of energy levels of the pyramidal quantum dot. The base width is $b = 15$ nm, the height $h = 7$ nm, the wetting layer width $d_{WL} = 1.7$ ML. The quantum number of total quasi-angular momentum m_f as well as the spin of each state is given. The unstrained GaAs conduction band edge was taken as the reference energy. The position of the wetting layer continuum and 3-D continuum states is indicated, as well.

states 2 and 3 in Fig. 3, while for larger energy separation the interaction with LO-phonons is dominant.

3) *Spontaneous Radiative Emission*: The transition rate from initial state i to final state f due to spontaneous emission of photons is given by [31]

$$W_{if} = \frac{(E_i - E_f)\bar{n}}{3\hbar^2 \epsilon_0 \pi c^3} \left(|\mathcal{M}_{e_x}|^2 + |\mathcal{M}_{e_y}|^2 + |\mathcal{M}_{e_z}|^2 \right). \quad (18)$$

The spontaneous radiative emission transition rates on the transition $2 \rightarrow 1$ for quantum dots whose dimensions are given in Table I, are shown in the inset of Fig. 2. We have found that the transition rates in the system due to spontaneous emission are less than $10 \mu s^{-1}$ and are thus significantly smaller than the transition rates due to interaction with phonons, hence they were neglected.

D. Laser Model

The rate equations for the system considered yield

$$\frac{dn_i}{dt} = \sum_{j \neq i} W_{ji} n_j \left(1 - \frac{1}{2} n_i \right) - \sum_{j \neq i} W_{ij} n_i \left(1 - \frac{1}{2} n_j \right) - \sum_j \sigma_{ij}^p(\omega_p) (n_i - n_j) \Phi \quad (19)$$

where $0 \leq n_i \leq 2$ is the occupancy of level i including electrons of both spin, W_{ij} is the total transition rate from state i to state j due to interaction with phonons, $\sigma_{ij}^p(\omega_p)$ is the optical cross section between states i and j at the pump wavelength for radiation polarized in the same way as the pump and Φ is the optical pump flux. The effect of final state blocking is included via the terms $(1 - (1/2)n_i)$ that represent the probability that the final state is empty.

It is assumed that the doping is such that there are n_d electrons per quantum dot on average, i.e., $\sum_i n_i = n_d$. An estimate based on solving the Poisson equation indicates that for the doping level considered in this work the electrostatic potential generated by donors can be neglected.

The dots considered here are in the strong confinement regime where the electron-electron interaction energy (which is of the order of ~ 10 meV per electron pair [32]) is much smaller than the effective confinement potential (which is ~ 500 meV). It is, therefore, expected that the single particle approach adopted here for the calculation of energy levels and the rate equations model should be valid when the dots are occupied by a small number of electrons ($n_d \sim 1-3$). This conclusion can also be supported by the results in [33] where the excitation spectrum of the quantum dot is almost the same in the range $n_d \sim 1-3$. Having all this in mind, a value of $n_d = 2$ was chosen in Section III to obtain large value of gain on one hand and to be sure in the validity of the model presented on the other hand.

The gain at the angular frequency ω for stimulated emission of radiation polarized in the direction ϵ is

$$g_\epsilon(\omega) = \sum_{\substack{i,j \\ E_i > E_j}} \sigma_{ij}^\epsilon(\omega) (n_i - n_j) N_t \quad (20)$$

where $\sigma_{ij}^\epsilon(\omega)$ is the optical cross section for interaction with radiation polarized in the direction ϵ and N_t is the number of quantum dots per unit of volume.

III. RESULTS

A. Active Region

We have first considered a quantum dot with a base width $b = 15$ nm, height $h = 7$ nm, and a wetting layer of width $d_{WL} = 1.7$ ML, which is a typical representative of the dots grown in experiments [26], [34]. It was assumed that the doping density is such that the dots are occupied with $n_d = 2$ electrons on average, as already mentioned. The material parameters for the calculation of the energy levels were taken from [35], the parameters for the calculation of transition rates due to interaction with phonons were taken from [36] and the temperature dependence of LO-phonon lifetime is taken from [28]. The energy level scheme of the dot considered is presented in Fig. 3.

Most of the optically pumped lasers use three-level or four-level schemes. We will however show that a somewhat more complicated scheme is required to obtain significant values of population inversion in the quantum dot investigated.

The standard three-level scheme would include pumping of electrons from level 1 to level 3, followed by fast depopulation of level 3 to level 2 in order to obtain a population inversion between levels 2 and 1. However, levels 2 and 3 are close in energy and, therefore, one cannot expect that selective pumping from level 1 to level 3 can be achieved in a real ensemble of quantum dots. We further note that electrons from level 1 cannot be pumped to level 4 or 6 due to selection rules for quantum number m_f and spin conservation.

Another possible pumping scheme would be to pump from level 1 to level 5. Electrons from level 5 then relax into levels 2 and 3 either directly or via level 4. In order to obtain a significant population inversion between levels 2 or 3, and level 1, the transition rate from level 5 to levels 2 and 3 should be much larger than the transition rate from levels 2 and 3 to level 1. However, these transition rates are of the same order of magnitude, the former being just slightly larger, hence our calculation has shown that only a small population inversion between levels 2 and 1 of approximately $\Delta n_{21} = n_2 - n_1 \approx 0.2$ electrons per dot at $T = 77$ K is possible. The main mechanism that prevents larger values of population inversions Δn_{21} or Δn_{31} is backfilling of level 1 by unavoidable stimulated emission of photons by electrons from level 5 (at the rate $\sigma_{15}\Phi(1 - (n_1/2))n_5$).

Therefore, we propose the following scheme which gives the largest values of gain among all the schemes explored. The electrons are optically pumped from level 1 to level 7. The distance between levels 5 and 7 is close to an LO-phonon energy and consequently the transition rate between these two levels exceeds all other LO-phonon interaction transition rates by more than an order of magnitude, enabling a fast depopulation of level 7. Consequently, the occupancy of level 7 in steady state is small and thus the undesirable stimulated emission from level 7 to level 1 is almost completely avoided in this scheme. The main difference between this and the previous scheme is that in this scheme there exists a fast depopulation mechanism from the level to which the electrons are being pumped, which prevents backfilling of level 1 by stimulated emission of photons. Almost all the electrons from level 7 therefore go into level 5, which implies that level 6 remains almost unpopulated. The electrons are further distributed to levels 2–4 and if the pump flux is sufficiently large, a population inversion between any of the levels 2–5 and level 1 occurs. As will be shown later, the largest population inversion occurs between levels 2 and 1, as well as between 3 and 1. Since the transition linewidth is of the same order of magnitude as the energy difference between states 2 and 3, laser emission is caused by both transitions $2 \rightarrow 1$ and $3 \rightarrow 1$. Due to selection rules on the transition $1 \rightarrow 7$, the pump needs to be z -polarized, while the emitted radiation is in-plane polarized, since the selection rules on both transitions $2 \rightarrow 1$ and $3 \rightarrow 1$ allow only such emission. Therefore, a laser based on these transitions can operate either as an edge emitter or as a surface emitter.

The rate equations were solved under steady-state conditions to find the population inversion and gain. The flux dependence

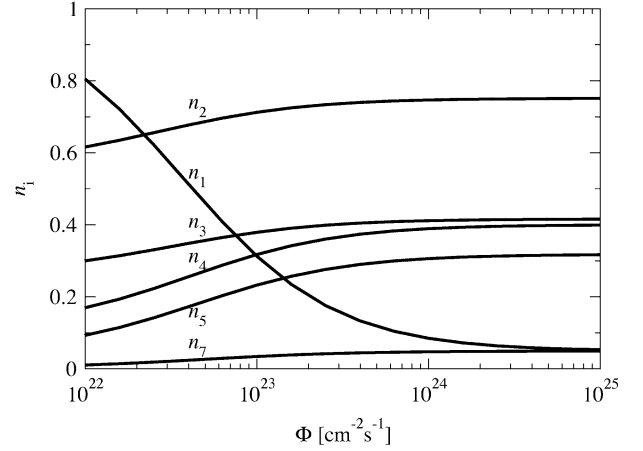


Fig. 4. Flux dependence of state occupancies n_i at a temperature $T = 77$ K for the quantum dot shown in Fig. 3.

of state occupancies n_i at a temperature $T = 77$ K are shown in Fig. 4. The population inversion between level 1 and any of the levels 2–5 appears at $\Phi \approx 2 \cdot 10^{23} \text{ cm}^{-2} \text{ s}^{-1}$. All the curves reach saturation at approximately $\Phi = 10^{24} \text{ cm}^{-2} \text{ s}^{-1}$. There are more electrons in levels 2 and 3 than in levels 4 and 5 since the transition rates from levels 4 and 5 to levels 2 and 3 are larger than the transition rates from levels 2 and 3 to level 1. This implies that the population inversion is strongest between levels 2 and 1 and the gain is, therefore, a maximum at the wavelength of $14.6 \mu\text{m}$, corresponding to the transition between levels 1 and 2. When the curves reach saturation, there is a population inversion of approximately 0.7 electrons per dot between levels 1 and 2 and 0.3 electrons between levels 1 and 3. Both of them contribute to the gain for in-plane polarized radiation at $\lambda_e \approx 14.6 \mu\text{m}$, which is calculated to be $g = 574 \text{ cm}^{-1}$. Our calculation shows that the dependence of the optical cross section on the direction of polarization in the xy -plane is weak and the above value of gain can be considered as the gain for any polarization direction of in-plane polarized radiation. It was assumed that the distance between quantum-dot planes is $L_z = 50 \text{ nm}$ and the surface density of dots was $N_s = 10^{11} \text{ cm}^{-2}$, which implies a quantum-dot density of $N_t = N_s/L_z = 2 \cdot 10^{16} \text{ cm}^{-3}$. At this point, we can *a posteriori* justify the approximation that continuum states are weakly occupied. One can see from Fig. 4. that among bound states only the levels 1–5 are significantly occupied. As the highest among them is 80 meV below the wetting layer continuum states (see Fig. 3), the electrons cannot be thermally excited to the continuum. The excitation to the continuum due to undesired absorption of pump photons by electrons from levels 2–5 is also negligible since the corresponding transition matrix elements between bound and continuum states are very small.

In order to emphasize the advantages of a quantum-dot intersublevel optically pumped laser over its quantum-well counterpart, we compare our results with the theoretical results for optimized optically pumped quantum-well lasers with smooth potential profile [37], emitting at a similar wavelength $\lambda \approx 15.5 \mu\text{m}$ as the device proposed here. At a pumping flux of $\Phi = 10^{24} \text{ cm}^{-2} \text{ s}^{-1}$ and a temperature $T = 77$ K the gain of the structure from [37] is less than 1 cm^{-1} , while the gain of our

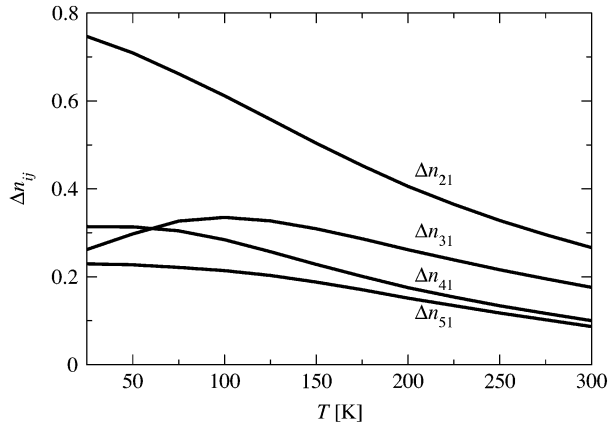


Fig. 5. Temperature dependence of population inversions $\Delta n_{i1} = n_i - n_1$ ($i \in \{2, 3, 4, 5\}$) at the pumping flux $\Phi = 10^{24} \text{ cm}^{-2} \text{ s}^{-1}$ for the quantum dot shown in Fig. 3.

structure is greater than 500 cm^{-1} . An order of magnitude larger flux is required there to obtain the same gain of $g \approx 570 \text{ cm}^{-1}$. Finally, the gain versus flux curve in [37] reaches saturation at $\Phi > 10^{26} \text{ cm}^{-2} \text{ s}^{-1}$, two orders of magnitude larger than in this work.

The temperature dependence of the population inversions between any of the levels 2–5 and level 1 $\Delta n_{i1} = n_i - n_1$ ($i \in \{2, 3, 4, 5\}$) at $\Phi = 10^{24} \text{ cm}^{-2} \text{ s}^{-1}$ is given in Fig. 5. An increase of Δn_{31} in the low temperature part of the graph is a consequence of the proximity of levels 2 and 3. The distribution of electrons between levels 2 and 3 here is in favor of the lower level 2. As the temperature increases, electrons become more evenly distributed between levels 2 and 3, thus increasing the population of level 3. When this trend reaches saturation, the decrease of Δn_{31} with temperature is caused by an increase in the population of the ground state. Due to an increase in the carrier relaxation rates to the ground state with temperature, the pumping flux is no longer sufficient to entirely depopulate the ground state at higher temperatures. Therefore, the population inversions Δn_{21} and Δn_{31} responsible for the gain decrease with temperature, but even at room temperature significant values of population inversions and gain are achievable.

In order to show that the dot analyzed is by no means an exception in view of the possibility of achieving significant values of gain, we have investigated several other dots of different sizes. The size, as well as the values of gain, the pump and the emission wavelength of the dots at the pumping flux $\Phi = 10^{24} \text{ cm}^{-2} \text{ s}^{-1}$ and the temperatures of $T = 77 \text{ K}$ and $T = 300 \text{ K}$ are shown in Table I. All the dots considered have values of gain larger than 400 cm^{-1} at $T = 77 \text{ K}$, and larger than 150 cm^{-1} at room temperature, and are thus obviously suitable for the active region of the laser in the proposed scheme.

The calculated gain profile for several different quantum dots with base-to-height ratio $b/h = 2$ at $T = 77 \text{ K}$ and $\Phi = 10^{24} \text{ cm}^{-2} \text{ s}^{-1}$ is shown in Fig. 6. In larger dots, the splitting between levels 2 and 3 is larger and the depopulation of level 3 to level 2 due to LA-phonon scattering is much

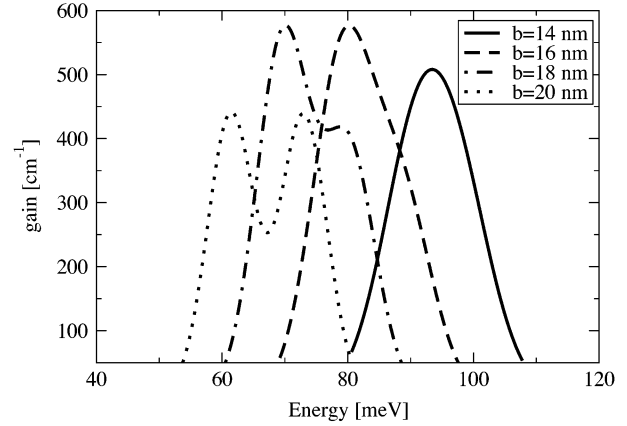


Fig. 6. Calculated gain profile for several different quantum dots with base-to-height ratio $b/h = 2$ at the temperature $T = 77 \text{ K}$ and the pumping flux $\Phi = 10^{24} \text{ cm}^{-2} \text{ s}^{-1}$.

smaller. Consequently, the electrons are more evenly distributed between levels 2 and 3, which results in a wider lineshape with two peaks and smaller values of peak gain for the larger dots, as shown in Fig. 6. This effect explains the decrease of gain as the dot size increases for larger ($b \sim 18\text{--}20 \text{ nm}$) dots at $T = 77 \text{ K}$ and consequently a smaller value of gain (see Table I) for the dot with $b = 20 \text{ nm}$ compared with other dots.

We should also note that either significantly smaller dots or dots with significantly larger base to height ratio than those investigated here cannot accommodate the required number of energy levels, and are not suitable for the proposed pumping scheme.

B. Waveguide and Cavity Design

We now consider the design of an appropriate waveguide, or of the resonator cavity, for either edge or surface emission, respectively. Since all the carriers in the proposed scheme are bound to quantum dots, the free carrier absorption can be neglected.

The waveguide for an edge emitting device may comprise a $5\text{-}\mu\text{m}$ -thick AIAs cladding layer, a $1\text{-}\mu\text{m}$ -thick GaAs core layer, 40 periods of quantum-dot layers (total thickness of $2 \mu\text{m}$) and a $2\text{-}\mu\text{m}$ -thick GaAs cap layer. For $\lambda = 14.6 \mu\text{m}$ this waveguide supports a single TM mode whose overlap with the active region is $\Gamma_{\text{TM}} = 52\%$ and a single TE mode whose overlap is $\Gamma_{\text{TE}} = 48\%$. Assuming the reflectivity $R \approx 0.29$ at the waveguide cleaved facets, the mirror losses for $l \approx 1 \text{ mm}$ long waveguide are $\alpha_M = -1/l \cdot \ln R \approx 13 \text{ cm}^{-1}$. The modal gain Γg is thus much larger than the losses, implying that edge emission from this laser is possible.

With the gain for normally incident light, the quantum-dot-based structure enables one to achieve VCSEL configuration, which would require an appropriate resonator. VCSELs operating at visible or near-infrared wavelengths perform very well and offer numerous advantages over edge emitters, but none has been fabricated for long wavelengths ($13\text{--}21 \mu\text{m}$), and this may be a quite challenging task. Here we briefly discuss a couple of possible routes of their realization.

One possibility might be to employ a cavity comprising two Bragg mirrors, based on GaAs–AlAs quarter-wavelength multilayer stack. The mirrors reflectivity is calculated from [38]

$$R = \frac{n_1^{2N} - n_2^{2N}}{n_1^{2N} + n_2^{2N}} \quad (21)$$

where n_1 and n_2 are the refractive indexes of GaAs and AlAs, and N is the number of bilayers. Assuming the active layer completely filling the resonator, and satisfying the proper phase condition $d = \lambda/(2n_1) \approx 2.2 \mu\text{m}$ i.e., comprising 44 layers of quantum dots, with interlayer spacing of $L_z = 50 \text{ nm}$, we find that the gain, even at room temperature, would exceed the equivalent mirror losses $\alpha_M = -1/d \cdot \ln R$ of an $N = 30$, or even $N = 20$ Bragg stack. A practical difficulty with this approach is that the total width of semiconductor layers is about $100 \mu\text{m}$, which makes it somewhat impractical for the whole structure to be grown by the slow molecular beam epitaxy (MBE) (the growth time might take a few days). A way out might be to employ the much faster liquid phase epitaxy (LPE) for the lower Bragg stack, polish the surface to prepare it for quantum dots growth, use MBE next, and finally make the upper Bragg stack by LPE. While the Bragg mirror performance might not be affected by $\sim 0.05 \mu\text{m}$ layer width tolerance/roughness inherent to LPE (because the $\lambda/4$ layer widths are here large), it is not quite clear whether the growth speed-up, at the expense of increased complexity, would make this approach practical.

The reasons for the Bragg mirrors being so thick are both the large operating wavelength, and a relatively small contrast of GaAs and AlAs refractive indices. While there is no cure for the former, the latter can be enhanced by wet-oxidation of AlAs layers into Al_2O_3 , the technique used for Bragg mirrors in the near-infrared [39]. With the smaller refractive index of Al_2O_3 we find that just $N = 7$ or 8 would suffice for lasing. It is not known, however, what losses would Al_2O_3 formed in this way present to the $13\text{--}21 \mu\text{m}$ radiation.

Yet another possibility is to employ metal mirrors, since the metal reflectance in this range is rather high, e.g., $\geq 97\%$ – 98% for Al, which suffices for lasing with $2\text{-}\mu\text{m}$ -thick active layer. In this case the total thickness of the structure is still likely to be large, mostly for the wafer handling reasons: one can think of a $\sim 100 \mu\text{m}$ GaAs substrate with an Al mirror deposited on its bottom, and the quantum-dot active layer grown on its top would then be covered by another $\sim 2 \mu\text{m}$ of GaAs spacer before depositing the upper Al mirror, to avoid having the optical field node near the active layer. This time, however, the major part of the thickness is due to the substrate, and should not result in excessive growth time. The outcoupling can be achieved by making a hole in the upper mirror (plane-parallel annular resonator).

In all of these layouts the relatively long resonator of the VCSEL demands for it to be wide enough to reduce the diffraction losses: e.g., $\leq 0.5\%$ losses require Fresnel number larger than 10, and hence the mirror diameter(s) of $\geq 150 \mu\text{m}$ for a $100 \mu\text{m}$ thick device.

IV. CONCLUSION

In conclusion, a theoretical model of the active region of an optically pumped intersublevel quantum-dot laser is presented.

The population of energy levels, and consequently the population inversion and gain were extracted from the rate equations model. The waveguide and cavity for edge and surface emission are proposed as well. Our results predict laser emission in the spectral range $13\text{--}21 \mu\text{m}$, depending on the dots size. The predicted threshold pumping flux, required to obtain laser action is much smaller than in quantum-well-based intersubband lasers, which is due to the longer carrier lifetimes in quantum dots.

REFERENCES

- [1] J. Faist, F. Capasso, D. L. Sivco, C. Sirtori, A. L. Hutchinson, and A. Y. Cho, "Quantum cascade laser," *Science*, vol. 264, pp. 553–556, 1994.
- [2] R. Köhler, A. Tredicucci, F. Beltram, H. E. Beer, E. H. Linfield, A. G. Davies, D. A. Ritchie, and R. C. Iotti, "Terahertz semiconductor-heterostructure laser," *Nature*, vol. 417, pp. 156–159, 2002.
- [3] O. Gauthier-Lafaye, P. Boucaud, F. H. Julien, S. Sauvage, S. Cabaret, J.-M. Lourtioz, V. Thierry-Mieg, and R. Planel, "Long-wavelength ($\approx 15.5 \mu\text{m}$) unipolar semiconductor laser in GaAs quantum wells," *Appl. Phys. Lett.*, vol. 71, pp. 3619–3621, 1997.
- [4] H. C. Liu and A. J. SpringThorpe, "Optically pumped intersubband laser: Resonance positions and many-body effects," *Phys. Rev. B*, vol. 61, pp. 15 629–15 632, 2000.
- [5] G. Sun and J. B. Khurgin, "Optically pumped 4-level infrared-laser based on intersubband transitions in multiple-quantum wells—Feasibility study," *IEEE J. Quantum Electron.*, vol. 29, no. 4, pp. 1104–1111, Apr. 1993.
- [6] N. Vukmirović, V. D. Jovanović, D. Indjin, Z. Ikonjić, P. Harrison, and V. Milanović, "Optically pumped terahertz laser based on intersubband transitions in a GaN/AlGaIn double quantum well," *J. Appl. Phys.*, vol. 97, p. 103 106, 2005.
- [7] N. S. Wingren and C. A. Stafford, "Quantum-dot cascade laser: Proposal for an ultralow-threshold semiconductor laser," *IEEE J. Quantum Electron.*, vol. 33, no. 7, pp. 1170–1173, Jul. 1997.
- [8] T. Inoshita and H. Sakaki, "Density of states and phonon-induced relaxation of electrons in semiconductor quantum dots," *Phys. Rev. B*, vol. 56, pp. R4355–R4358, 1997.
- [9] S. Hameau, Y. Guldner, O. Verzelien, R. Ferreira, G. Bastard, J. Zeman, A. Lemaître, and J. M. Gérard, "Strong electron-phonon coupling regime in quantum dots: Evidence for everlasting resonant polarons," *Phys. Rev. Lett.*, vol. 83, pp. 4152–4155, 1999.
- [10] X.-Q. Li, H. Nakayama, and Y. Arakawa, "Phonon bottleneck in quantum dots: Role of lifetime of the confined optical phonons," *Phys. Rev. B*, vol. 59, pp. 5069–5073, 1999.
- [11] O. Verzelien, R. Ferreira, and G. Bastard, "Polaron lifetime and energy relaxation in semiconductor quantum dots," *Phys. Rev. B*, vol. 62, pp. R4809–R4812, 2000.
- [12] J. Urayama, T. B. Norris, J. Singh, and P. Bhattacharya, "Observation of phonon bottleneck in quantum dot electronic relaxation," *Phys. Rev. Lett.*, vol. 86, pp. 4930–4933, 2001.
- [13] S. Sauvage, P. Boucaud, R. P. S. M. Lobo, F. Bras, G. Fishman, R. Prazeres, F. Glotin, J. M. Ortega, and J.-M. Gérard, "Long polaron lifetime in InAs–GaAs self-assembled quantum dots," *Phys. Rev. Lett.*, vol. 88, p. 177 402, 2002.
- [14] C.-F. Hsu, J.-S. O, P. Zory, and D. Botez, "Intersubband quantum-box semiconductor lasers," *IEEE J. Sel. Topics Quantum Electron.*, vol. 6, no. 3, pp. 491–503, May/June 2000.
- [15] V. M. Apalkov and T. Chakraborty, "Luminescence spectra of a quantum-dot cascade laser," *Appl. Phys. Lett.*, vol. 78, pp. 1820–1822, 2001.
- [16] I. A. Dmitriev and R. A. Suris, "Quantum cascade lasers based on quantum dot superlattice," *Phys. Stat. Sol. A*, vol. 202, pp. 987–991, 2005.
- [17] S. Anders, L. Rebohle, F. F. Schrey, W. Schrenk, K. Unterrainer, and G. Strasser, "Electroluminescence of a quantum dot cascade structure," *Appl. Phys. Lett.*, vol. 82, pp. 3862–3864, 2003.
- [18] N. Ulbrich, J. Bauer, G. Scarpa, R. Boy, D. Schuh, G. Abstreiter, S. Schmult, and W. Wegscheider, "Midinfrared intraband electroluminescence from AlInAs quantum dots," *Appl. Phys. Lett.*, vol. 83, pp. 1530–1532, 2003.
- [19] N. Vukmirović, D. Indjin, V. D. Jovanović, Z. Ikonjić, and P. Harrison, "Symmetry of $k \cdot p$ Hamiltonian in pyramidal InAs/GaAs quantum dots: Application to the calculation of electronic structure," *Phys. Rev. B*, vol. 72, pp. 075356/1–075366/10, 2005.

- [20] T. B. Bahder, "Eight-band $k \cdot p$ model of strained zinc-blende crystals," *Phys. Rev. B*, vol. 41, pp. 11 992–12 001, 1990.
- [21] A. D. Andreev and E. P. O'Reilly, "Theory of the electronic structure of GaN/AlN hexagonal quantum dots," *Phys. Rev. B*, vol. 62, pp. 15 851–15 870, 2000.
- [22] A. D. Andreev, J. R. Downes, D. A. Faux, and E. P. O'Reilly, "Strain distributions in quantum dots of arbitrary shape," *J. Appl. Phys.*, vol. 86, pp. 297–305, 1999.
- [23] Z. Ikončić, V. Milanović, and M. Tadić, "Intersubband optical-transition matrix-elements for hole states in semiconductor quantum-wells," *J. Phys.: Condens. Matter*, vol. 7, pp. 7045–7052, 1995.
- [24] E. Towe and D. Pan, "Semiconductor quantum-dot nanostructures: Their application in a new class of infrared photodetectors," *IEEE J. Sel. Topics Quantum Electron.*, vol. 6, no. 3, pp. 408–421, May/June 2000.
- [25] J.-Z. Zhang and I. Galbraith, "Intraband absorption for InAs–GaAs quantum dot infrared photodetectors," *Appl. Phys. Lett.*, vol. 84, pp. 1934–1936, 2004.
- [26] D. Bimberg, M. Grundmann, and N. N. Ledentsov, *Quantum Dot Heterostructures*. Chichester, U.K.: Wiley, 1999.
- [27] T. R. Nielsen, P. Gartner, and F. Jahnke, "Many-body theory of carrier capture and relaxation in semiconductor quantum-dot lasers," *Phys. Rev. B*, vol. 69, p. 235 314, 2004.
- [28] A. R. Bhat, K. W. Kim, and M. A. Strosio, "Theoretical calculation of longitudinal-optical-phonon lifetime in GaAs," *J. Appl. Phys.*, vol. 76, pp. 3905–3907, 1994.
- [29] L. F. Register, "Microscopic basis for a sum rule for polar-optical-phonon scattering of carriers in heterostructures," *Phys. Rev. B*, vol. 45, pp. 8756–8759, 1992.
- [30] E. A. Zibik, L. R. Wilson, R. P. Green, G. Bastard, R. Ferreira, P. J. Phillips, D. A. Carder, J.-P. R. Wells, J. W. Cockburn, M. S. Skolnick, M. J. Steer, and M. Hopkinson, "Intraband relaxation via polaron decay in InAs self-assembled quantum dots," *Phys. Rev. B*, vol. 70, p. 161 305, 2004.
- [31] H. Jiang and J. Singh, "Self-assembled semiconductor structures: Electronic and optoelectronic properties," *IEEE J. Quantum Electron.*, vol. 34, no. 7, pp. 1188–1196, Jul. 1998.
- [32] L. R. C. Fonseca, J. L. Jimenez, J. P. Leburton, and R. M. Martin, "Self-consistent calculation of the electronic structure and electron-electron interaction in self-assembled InAs–GaAs quantum dot structures," *Phys. Rev. B*, vol. 57, pp. 4017–4026, 1998.
- [33] A. Wojs and P. Hawrylak, "Charging and infrared spectroscopy of self-assembled quantum dots in a magnetic field," *Phys. Rev. B*, vol. 53, pp. 10 841–10 845, 1996.
- [34] T. Nakaoka, T. Saito, J. Tatebayashi, and Y. Arakawa, "Size, shape and strain dependence of the g factor in self-assembled In(Ga)As quantum dots," *Phys. Rev. B*, vol. 70, p. 235 337, 2004.
- [35] I. Vurgaftman, J. R. Meyer, and L. R. Ram-Mohan, "Band parameters for III-V compound semiconductors and their alloys," *J. Appl. Phys.*, vol. 89, pp. 5815–5867, 2001.
- [36] G. Shkerdin, J. Stiens, and R. Vounckx, "Hot free-electron absorption in nonparabolic III-V semiconductors at midinfrared wavelengths," *J. Appl. Phys.*, vol. 85, pp. 3792–3806, 1999.
- [37] S. Tomić, M. Tadić, V. Milanović, and Z. Ikončić, "The optimization of optical gain in the intersubband quantum well laser," *J. Appl. Phys.*, vol. 87, pp. 7965–7972, 2000.
- [38] E. Rosencher and B. Vinter, *Optoelectronics*. Cambridge, MA: Cambridge University Press, 2002.
- [39] D. J. Ripin, J. T. Gopinath, H. M. Shen, A. A. Erchak, G. S. Petrich, L. A. Kolodziejski, F. X. Kärtner, and E. P. Ippen, "Oxidized GaAs/AlAs mirror with a quantum well saturable absorber for ultrashort-pulse Cr^{4+} :YAG laser," *Opt. Commun.*, vol. 214, pp. 285–289, 2002.



Nenad Vukmirović (S'05) was born in Belgrade, Serbia, in 1980. He received the B.Sc. degree in physics in 2003, and the B.Sc. degree in electrical engineering in 2004, both from the University of Belgrade, Belgrade, Serbia. He is currently pursuing the Ph.D. degree at the Institute of Microwaves and Photonics, School of Electronic and Electrical Engineering, University of Leeds, Leeds, U.K., in the field of quantum-dot optoelectronic devices.

As a high school student, Mr. Vukmirović won the gold medal at the International Physics Olympiad in

1999. He is a member of the Editorial Board of the *Young Physicist*, a physics journal for elementary and high school students.



Zoran Ikončić was born in Belgrade, Yugoslavia, in 1956. He received the B.Sc., M.Sc., and Ph.D. degrees in electrical engineering from the University of Belgrade, Yugoslavia, in 1980, 1984, and 1987, respectively.

From 1981 to 1999, he has been with the Faculty of Electrical Engineering, University of Belgrade (Full Professor from 1998). In 1999, he joined the Institute of Microwaves and Photonics, University of Leeds, Leeds, U.K. His research interests include the electronic structure, optical and transport properties of semiconductor nanostructures, and devices based upon them.



Vladimir D Jovanović was born in Belgrade, Yugoslavia, in 1978. He received the B.Sc. degree in electrical engineering from the University of Belgrade, Belgrade, Yugoslavia, in 2002 and the Ph.D. degree from the Institute of Microwaves and Photonics, School of Electronic and Electrical Engineering, University of Leeds, Leeds, U.K., in 2005, focused on physical modeling, design and optimization of quantum-well infrared photodetectors and quantum cascade lasers in GaN- and GaAs-based materials for near-, midinfrared, and

terahertz applications.

Dr. Jovanović is a Laureate of the prestigious IEE Leslie H. Paddle Fellowship, and received the SPIE Educational Awards in 2004 and again in 2005.



Dragan Indjin was born in Zemun, Yugoslavia, in 1963. He received the B.Sc., M.Sc., and Ph.D. degrees in electrical engineering from the University of Belgrade, Yugoslavia, in 1988, 1993, and 1996, respectively.

From 1989 to 2001, he was with the Faculty of Electrical Engineering, University of Belgrade, where he held the position of Associate Professor. In 2001, he joined the Institute of Microwaves and Photonics, School of Electronic and Electrical Engineering, University of Leeds, Leeds, U.K., where

he has recently obtained the prestigious Academic Fellowship. His research interests include the electronic structure, optical and transport properties, optimization and design of quantum wells, superlattices, quantum cascade lasers and quantum-well infrared photodetectors from near- to far-infrared spectral range.



Paul Harrison (SM'99) received the B.Sc. degree from the University of Hull, Hull, U.K., in 1988, and the Ph.D. degree from the University of Newcastle-upon-Tyne, U.K., in 1991.

He was a Postdoctoral Research Assistant at the University of Hull until 1995, when he obtained a Fellowship at the University of Leeds, Leeds, U.K. Since joining the Institute of Microwave and Photonics, University of Leeds, he has been working on ways to adapt his theoretical and computational experience in semiconductor heterostructures to

terahertz sources and detectors. He currently holds a chair in Quantum Electronics and is Head of the School of Electronic and Electrical Engineering. He is author of the book *Quantum Wells, Wires and Dots, Second Edition* (Chichester, U.K.: Wiley, 2005).